Local $\mathcal{PT}$ invariance and supersymmetric parametric oscillators

Ramy El-Ganainy,[1] Konstantinos G. Makris,[2] and Demetrios N. Christodoulides[3]
[1]*Department of Physics, University of Toronto, 60 St. George Street, Toronto, Ontario, Canada M5S 1A7*
[2]*Department of Electrical Engineering, Princeton University, Princeton, New Jersey 08544, USA*
[3]*College of Optics/CREOL, University of Central Florida, Orlando, Florida 32816, USA*
(Received 14 April 2012; published 11 September 2012)

We introduce the concept of local parity-time symmetric ($\mathcal{PT}$) invariance in optical waveguides (or cavity) structures. Starting from a Lagrangian formalism, we establish the connection between light dynamics in these configurations and the seemingly different physics of "supersymmetric" parametric oscillators. Using this powerful tool, we present analytical solutions for optical beam propagation in local $\mathcal{PT}$-invariant coupled systems and we show that the intensity tunneling between the two channels critically depends on the initial conditions. For unbalanced inputs, symmetric as well as asymmetric power evolution can be observed depending on the excitation channel. On the other hand, under certain physical conditions, our analysis predicts that for a modal $\mathcal{PT}$-symmetric input, a unidirectional fractional phase exchange can take place. Few cases where analytical solutions cease to exist are also investigated numerically. Finally, by exploiting the supersymmetric nature of the oscillator equations, we show that under certain initial conditions, one can obtain the propagation dynamics of field amplitudes that "resides" on the supersymmetric eigenfunctions of the system—a phenomenon we call resonant propagation.

DOI: 10.1103/PhysRevA.86.033813 PACS number(s): 42.25.Hz, 42.82.Et, 42.25.Fx

I. INTRODUCTION

Parity-time ($\mathcal{PT}$) symmetric Hamiltonian systems have attracted considerable attention in the past decade. This interest arose after the seminal work of Bender *et al.* [1], who first suggested that a certain class of $\mathcal{PT}$-symmetric Hamiltonian operators can exhibit entirely real eigenvalue spectra. This is indeed a counterintuitive result given that in general these Hamiltonians are not Hermitian. Moreover, such systems can experience a sudden phase transition, better known as spontaneous $\mathcal{PT}$-symmetry breaking [1,2]. Above this critical threshold the spectrum ceases to be real and the eigenvalues can spread over the entire complex plane [1–4]. Within the framework of the Schrödinger picture, $\mathcal{PT}$ symmetry arises as a direct outcome of complex potentials exhibiting symmetric and antisymmetric real and imaginary parts, respectively. While the Hermiticity of quantum mechanics was never in doubt, the formal analogy between the Schrödinger equation and the paraxial equation of diffraction was recently exploited to introduce for the first time the notion of $\mathcal{PT}$ symmetry within the context of optical physics [5–9]. Parity-time symmetry in optics can be realized by introducing a complex refractive index profile having an even space guiding index (real part) distribution, while the gain or loss (imaginary part) component is odd. In analogy with their $\mathcal{PT}$-symmetric Hamiltonian counterparts, these optical structures were shown to exhibit real eigenvalue spectra and phase transitions [5,6]. Quite recently, $\mathcal{PT}$-symmetric behavior and dynamics were experimentally observed in optical systems [10,11]. Moreover, a new family of optical isolators that exploits the interplay between optical nonlinearities and nonreciprocal $\mathcal{PT}$ behavior was also proposed [12]. It is important to note that in all the above-mentioned studies, the investigated configurations were assumed to exhibit global $\mathcal{PT}$ symmetry in the transverse direction, while being uniform in the propagation direction or stationary with time. In other words, along the evolution direction (distance z or time t), the aforementioned systems exhibit this symmetry in a z/t-invariant fashion. Lately, $\mathcal{PT}$-symmetric two-level time periodic systems were investigated where the levels crossing rules were analyzed [13] and adiabatic evolution in non-Hermitian Hamiltonians with isolated degeneracies was investigated [14]. Time-dependent dissipative nonlinear Bose-Einstein systems were also studied and nonlinear Zeno effects were reported [15].

Another seemingly independent and different line of research is that of parametric oscillations (PO). This process (PO) represents a very general phenomenon and can be observed in wide varieties of physical systems [16–18]. Mechanical pendulums and springs, electric circuits, and optical devices are just a few examples in which PO were thoroughly studied. The underlined principle of PO in all the above-mentioned systems is well understood and can be viewed as oscillations taking place under the action of time-dependent parameters. PO has found a broad range of applications, from microwave electronics [19] to frequency mixing in optics [20]. A closely related phenomenon is parametric amplification (PA), also widely used in many areas of engineering [19,20]. Many interesting effects emerge from the physics of PO. For instance, parametrically driven systems exhibit a special type of resonance, naturally called parametric resonance. Also, as opposed to linearly forced oscillators, parametric ones demonstrate some nonlinear characteristics such as instabilities, for example.

In this work, we consider optical coupled systems exhibiting an even distribution and an antisymmetric profile for the real and imaginary parts of the complex refractive index profiles when the gain-loss distributions are also a function of the propagation distance or evolution time, i.e., they exhibit z or t dependence. In these configurations, as long as the index guiding is even and the gain-loss arrangement remains odd at every propagation distance or time step, we say that the system exhibits *local $\mathcal{PT}$ symmetry* (see Fig. 1).

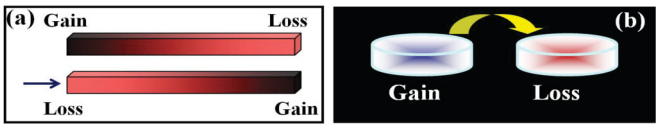

FIG. 1. (Color online) Schematics of local $\mathcal{PT}$-symmetric coupled waveguides (a) and cavities (b).

In Sec. II we establish the mathematical equivalence of parametric oscillations and local $\mathcal{PT}$ systems. Starting from a Lagrangian formalism for a parametric oscillator, we derive the system's Hamiltonian and we show that through a proper choice of the canonical variables, the equation of motion reduces to that of local $\mathcal{PT}$-symmetric coupled systems. It is worth noting that the analogies between photonic structures with modulated parameters and parametric systems were discussed in previous publications [21] where the authors demonstrated parametric amplification of soliton steering in modulated optical lattices.

A specific example of local $\mathcal{PT}$-symmetric coupled waveguide systems is investigated in Sec. III where we consider different scenarios of the input power excitations. We show that, depending on the initial conditions, the dynamics of intensity evolution can vary considerably. For example, by exciting only the initial gain or loss arm, our work indicates different dynamics where certain symmetry emerges in one case and is lacking in the other. We also investigate what happens when the input beam is a $\mathcal{PT}$-symmetric mode. In such situation, our analysis reveals an interesting property related to the evolution of the optical beam phase. As we will see, while the normalized phase in one arm varies with propagation, the phase in the other channel remains constant—a process here we call unidirectional phase exchange.

In Sec. IV, we highlight the connection between local $\mathcal{PT}$ optical structures and supersymmetry (SUSY) in quantum mechanics. More specifically, we investigate situations where the coupling constant values are chosen from a specific discrete set of values that correspond to solutions of stationary Schrödinger equations with SUSY-related potentials. We show that carefully tailored inputs will evolve residing on the corresponding set of eigenfunctions.

II. PARAMETRIC OSCILLATIONS AND LOCAL $\mathcal{PT}$ SYMMETRY

We start our analysis by considering a parametric harmonic oscillator described by

$$\ddot{x} + 2\gamma(\xi)\dot{x} + \omega^2 x = 0, \tag{1}$$

where $\dot{x} = dx/d\xi$, ξ stands for time t (or as we will see later, propagation distance z), $\gamma(\xi)$ is a time (distance)-varying friction (or gain), and ω is the natural frequency of the oscillator. The Lagrangian associated with the above equation is given by [22]

$$\tilde{L} = \tfrac{1}{2}M(\xi)\dot{x}^2 - \tfrac{1}{2}M(\xi)\omega^2 x^2. \tag{2}$$

A direct substitution in the Euler-Lagrange equation $(d/d\xi)(\partial\tilde{L}/\partial\dot{x}) - (\partial\tilde{L}/\partial x) = 0$ yields Eq. (1) with $2\gamma = \dot{M}/M$. Next we use the standard transformation $x = Dq$, where q is a new coordinate variable and $D = \exp(-\int_0^\xi \gamma(\xi')d\xi') = 1/\sqrt{M}$. Accordingly, Eq. (1) becomes

$$\ddot{q} + [\omega^2 - \dot{\gamma}(\xi) - \gamma^2(\xi)]q = 0, \tag{3}$$

and the new Lagrangian takes the form

$$\tilde{L} = \tfrac{1}{2}(\dot{q}^2 - 2\gamma q\dot{q}) - \tfrac{1}{2}(\omega^2 - \gamma^2)q^2. \tag{4}$$

Let us define p to be the conjugate momentum for the variable q. It follows that

$$p = \frac{\partial\tilde{L}}{\partial\dot{q}} = \dot{q} - \gamma q, \tag{5a}$$

$$\tilde{H} = p\dot{q} - \tilde{L} = \frac{p^2}{2} + \gamma pq + \frac{\omega^2}{2}q^2. \tag{5b}$$

In Eq. (5b), $\tilde{H}$ is the system's Hamiltonian. So far, our analysis is only restricted for real coordinates and momenta, but in principle, one can solve the parametric oscillation problem using real as well as complex functions. In order to establish the connection with local $\mathcal{PT}$-symmetric systems, we need to write down a Lagrangian that would allow for complex canonical variables:

$$L = \dot{q}\dot{q}^* - (\omega^2 - \gamma^2)qq^* - \gamma(q\dot{q}^* + q^*\dot{q}). \tag{6}$$

One can immediately check that $\delta L/\delta q^*$ gives the equation of motion (3), while $\delta L/\delta q$ reduces to the complex conjugate of Eq. (3). The new Hamiltonian defined as $H = p\dot{q} + p^*\dot{q}^* - L$ is given by

$$H = pp^* + \gamma(pq + p^*q^*) + \omega^2 qq^*, \tag{7}$$

where in Eq. (7), $p = \partial L/\partial\dot{q} = \dot{q}^* - \gamma q^*$ and $p^* = \partial L/\partial\dot{q}^* = \dot{q} - \gamma q$.

The equation of motion for the canonical momentum can be found by using Hamilton's equations: $\dot{p} = \partial p/\partial\xi + \{p, H\}$, where the Poisson brackets are given by $\{A, B\} = (\partial A/\partial q)(\partial B/\partial p) - (\partial A/\partial p)(\partial B/\partial q)$. By doing so, we obtain $\dot{p} + \gamma\, p + \omega^2 q^* = 0$. By using the substitution $q^* = b$ and scaling the momentum $p = i\omega a$, the above formula, together with the relation $p^* = \dot{q} - \gamma q$ gives:

$$i\dot{a} + i\gamma(\xi)a + \omega b = 0, \tag{8a}$$

$$i\dot{b} - i\gamma(\xi)b + \omega a = 0. \tag{8b}$$

These are the equations of motion for the scaled canonical coordinate b and the variable a which is proportional to the canonical momentum.

Note that the gain-loss profile of Eqs. (8) is always antisymmetric irresepective of the value of $\gamma(\xi)$ and hence the second-order parametric harmonic oscillator is reduced to two first-order local $\mathcal{PT}$-symmetric coupled configurations. Equations (8) can be used, for example, to describe the physics of two coupled waveguides (cavities) with an asymmetric gain-loss profile that varies with distance (time) as shown in Fig. 1. This unexpected connection opens the door for taking a fresh look at the behavior of PO through the properties of $\mathcal{PT}$ symmetry and for establishing a link between two seemingly different physical systems. The decoupling of the above system of first-order differential equations will result in Eq. (3) and

another equation for p:

$$\ddot{p} + [\omega^2 + \dot{\gamma}(\xi) - \gamma^2(\xi)]p = 0. \tag{9}$$

It is important to note the structure of the time- or distance-dependent parts of the natural frequency components in both Eq. (3) and Eq. (9). They are related via the same relationship that defines supersymmetric (SUSY) potentials in quantum mechanics [23]. That is to say, if one considers Eqs. (3) and (8) as stationary Schrödinger equations, ω^2 will play the role of the eigenvalues and $\dot{\gamma}(\xi) \pm \gamma^2(\xi)$ will be the potential. This form of the potential with the plus-minus sign defines supersymmetry (SUSY) in quantum mechanics [24]. This observation has important implications in constructing mathematical solutions for "supersymmetric" parametric oscillator problems. In addition, as will be shown later, it leads to altogether new dynamics.

At this point, we examine the conserved quantities of the first-order system in Eqs. (8). We first define the usual Stokes parameters $S_0 = |a|^2 + |b|^2$, $S_1 = |a|^2 - |b|^2, S_2 = ab^* + a^*b, S_3 = i(ab^* - ab^*)$. First we examine the situation when γ is constant. In such situation one can verify by direct substitution that the system exhibit two constants of motions: $J_1 = \omega S_0 + \gamma S_3$ and $J_2 = S_2$. Note that for $\gamma = 0$, $J_1 = \omega S_0$, i.e. up to a constant factor, it reduces to S_0 as expected. It is instructive to understand the origin of these invariant quantities using the parametric oscillator formalism. Of course when the gain-loss profile is constant, the problem reduces to that of a harmonic oscillator and we note that the Lagrangian of the system (6) becomes ξ independent. It follows immediately from Noether's theorem that the Hamiltonian of Eq. (7) is a conserved quantity. Expressing the Hamiltonian in terms of the new variables a and b, we find that in this case $H = \omega(\omega S_0 + \gamma S_3) = \omega J_1$. Thus we identify J_1 as the constant of motion that corresponds to distance (or time) translation symmetry. It is an external symmetry of the system when $\gamma =$ const. and obviously it breaks down when the gain-loss profile varies with ξ.

On the other hand, the second quantity J_2 is always conserved, even when $\gamma = \gamma(\xi)$ and thus it must be connected to a stronger symmetry that is not violated by varying the gain-loss profile. By investigating the form of the Lagrangian of Eq. (6), we find that it exhibits global gauge symmetry under the action of the U(1) group. In other words, it is invariant under the transformation $q \to qe^{i\alpha}$, where α is a continuous real parameter. If one considers small α we find that $dq \to i\alpha q$ and the change in the Lagrangian becomes $dL = 0 = (\partial L/\partial q)dq + (\partial L/\partial \dot{q})d\dot{q} + (\partial L/\partial q^*)dq^* + (\partial L/\partial \dot{q}^*)d\dot{q}^*$. By using $dq \to i\alpha q$, dL can be written as

$$dL = i\alpha \left\{ \left[\frac{\partial L}{\partial q} - \frac{d}{d\xi}\left(\frac{\partial L}{\partial \dot{q}}\right)\right] q - \left[\frac{\partial L}{\partial q^*} - \frac{d}{d\xi}\left(\frac{\partial L}{\partial \dot{q}^*}\right)\right] q^* \right\} + i\alpha \frac{d}{d\xi}\left\{ \frac{\partial L}{\partial \dot{q}} q - \frac{\partial L}{\partial \dot{q}^*} q^* \right\} = 0.$$

The terms inside the first two brackets are recognized as the Euler-Lagrange equations and they are identically zero and we are thus left with $(d/d\xi)\{(\partial L/\partial \dot{q})q - (\partial L/\partial \dot{q}^*)q^*\} = 0$, i.e., the quantity $Q = \{(\partial L/\partial \dot{q})q - (\partial L/\partial \dot{q}^*)q^*\}$ is conserved [25]. In the context of quantum field theories, this constant of motion is termed the Noether current. A direct substitution shows that $Q = \dot{q}^*q - \dot{q}q^* = pq - p^*q^*$. In terms of the variables a and b, $Q = i\omega(ab^* + a^*b) = i\omega J_2$. Thus we see that the invariance of J_2 is a direct outcome of the internal U(1) gauge symmetry. Typically, in the context of $\mathcal{PT}$ symmetry, J_2 is termed the "quasipower," however, our analysis suggests that it might be more adequate to reserve this term for J_1 and use "$\mathcal{PT}$ current" for J_2 instead.

III. $\mathcal{PT}$-INVARIANT OPTICAL COUPLED STRUCTURES

So far our discussion on the connection between local $\mathcal{PT}$ symmetry and parametric oscillations has been general and can be applied to any distance- or time-dependent gain-loss profile. In order to gain further insight into the dynamical evolution of the system, here we consider a specific example of local $\mathcal{PT}$ symmetry that admits an analytical solution. We focus our attention on the coupled waveguide system shown in Fig. 1(a) and we consider the case where the gain-loss profile $\gamma(z)$ varies with propagation distance, while the coupling $\kappa = \kappa_0$ is constant.

Within the framework of coupled mode theory, the structure under consideration can be described by a set of differential equations similar to those of Eq. (8):

$$i\frac{da}{dz} + i\gamma(z)a + \kappa_0 b = 0, \tag{10a}$$

$$i\frac{db}{dz} - i\gamma(z)b + \kappa_0 a = 0. \tag{10b}$$

In Eq. (10) a and b are the electric field amplitudes in the two different coupled channels. Note that in general, the above system might not possess $\mathcal{PT}$ symmetry in the rigorous sense. However, as we explained before, since the gain-loss profile satisfies the antisymmetric property at every point z, the system is said to exhibit local $\mathcal{PT}$ symmetry. The above equations can also be used to describe optical $\mathcal{PT}$-symmetric cavities where in this case the coordinate z is replaced by the time variable t. Figure 1(b) depicts a schematic for such geometries.

As has been pointed out previously, the coupled mode equations are equivalent to a set of two "supersymmetric" parametric oscillators:

$$\ddot{a} + \left(\kappa_0^2 - \gamma^2 + \dot{\gamma}\right)a = 0, \tag{11a}$$

$$\ddot{b} + \left(\kappa_0^2 - \gamma^2 - \dot{\gamma}\right)b = 0, \tag{11b}$$

where $\dot{a} = da/dz$, etc. Equations (11a) and (11b) are not independent; instead they are linked through Eqs. (10). Thus it is only sufficient to solve either one of Eqs. (11) and then deduce the rest of the solution from Eq. (10a) or Eq. (10b).

Here we take $\gamma(z) = W \tanh(Wz) = WT(z)$, where W is a constant and $T(z) = \tanh(Wz)$. Note that the gain-loss distribution is antisymmetric with respect to z. In the regime where $W > \kappa_0$, the $\mathcal{PT}$ symmetry is broken and the system will experience total net exponential gain or loss depending on the details of the gain-loss variations and the input initial conditions. Here we consider only the case of $W < \kappa_0$, where local $\mathcal{PT}$-symmetry breaking never occurs along z. Under these conditions, Eq. (11b) reduces to that of a simple harmonic oscillator, e.g., $\ddot{b} + \lambda^2 b = 0$ with $\lambda^2 = \kappa_0^2 - W^2$. The dynamics of this system is obtained by solving the above equation in conjunction with Eq. (10b).

We first analyze the case when the optical input enters the channel exhibiting loss as shown in Fig. 1(a). We assume the length of the coupled structure is $2z_0$ and we chose our coordinates such that the system extends from $-z_0$ to z_0. Under the initial conditions $a(-z_0) = 0$ and $b(-z_0) = b_0$, the field amplitudes in both arms are given by

$$b = b_0 \left\{ \cos\left[\lambda\left(z + z_0\right)\right] - \frac{WT_0}{\lambda} \sin\left[\lambda\left(z + z_0\right)\right] \right\}, \quad (12a)$$

$$a = \frac{ib_0}{\kappa_0} \left\{ W\left[T_0 + T(z)\right] \cos\left[\lambda\left(z + z_0\right)\right] + \left(\lambda - \frac{W^2 T_o}{\lambda} T(z)\right) \sin\left[\lambda\left(z + z_0\right)\right] \right\}, \quad (12b)$$

where in the above expression, $T_0 = \tanh(Wz_0)$. Note that both z_0 and T_0 are positive quantities.

In the opposite scenario when the beam is excited from the gain channels, i.e., $a(-z_0) = a_0$ and $b(-z_0) = 0$, the optical wave evolves according to

$$b = a_0 \frac{i\kappa_0}{\lambda} \sin\left[\lambda\left(z + z_0\right)\right], \quad (13a)$$

$$a = a_0 \left\{ \cos\left[\lambda\left(z + z_0\right)\right] - \frac{W}{\lambda} T(z) \sin\left[\lambda\left(z + z_0\right)\right] \right\}. \quad (13b)$$

Figures 2(a) and 2(b) show a plot of the intensities $|a|^2$ and $|b|^2$ in both of these scenarios, respectively. The blue and red lines represent optical power in the loss and gain channels, correspondingly.

In both cases tunneling between the two channels occurs in an oscillatory fashion. Power oscillations are also observed, which is a characteristic of $\mathcal{PT}$-symmetric systems [6–9]. However, the coupling dynamics are quite different for these two cases. In the first case the intensity initially experiences loss, while in the second situation gain takes over at the beginning of the cycle. This result is expected given the exact character of gain-loss distribution in our specific example. As shown in Figs. 2(a) and 2(b), a phase shift takes place around the axis of symmetry (shown by a green dotted line). This is clearly manifested by the order of the leading peaks before and after that center line. An important difference, however, is that in Fig. 2(b), the intensity evolution as a function of z is symmetric around the middle axis. The absence of this feature from Fig. 2(a) can also be understood through the analytical solutions presented in Eqs. (12). In all the above, as well as the following simulations, the parameters of the coupled $\mathcal{PT}$ structure were chosen to be $\kappa_0 = 0.7$ and $W = 0.5$.

We also examine the case when both channels are excited with the local modal $\mathcal{PT}$ -symmetric eigenvector (stationary solution at the input waveguide in the absence of z modulation), i.e., when $a(-z_0) = e^{-i\theta}$ and $b(-z_0) = 1$, where $\tan(\theta) = WT_0/\sqrt{\kappa_0^2 - W^2T_0^2}$. Substituting these values for a and b into the general solution of the harmonic equation, we find that

$$b = \cos\left[\lambda\left(z + z_0\right)\right] + i\sigma \sin\left[\lambda\left(z + z_0\right)\right], \quad (14a)$$

$$a = \frac{i}{\kappa_o}\{[WT(z) - i\sigma\lambda]\cos[\lambda(z + z_0)] + i\left[\sigma WT(z) - i\lambda\right]\sin[\lambda(z + z_0)]\}. \quad (14b)$$

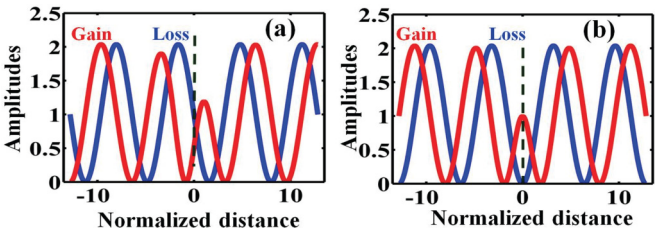

FIG. 2. (Color online) Tunneling dynamics when the input beam initially excites (a) the lossy and (b) the gain channel. Blue (red) color represents initially loss (gain) arms. The dashed green line marks the axis of time symmetry for $\gamma(z)$. The curves representing light evolution in initially loss-gain channels are indicated in the figure.

In Eqs. (14), $\sigma = \sqrt{\kappa_0^2 - W^2T_0^2}/\sqrt{\kappa_0^2 - W^2}$. It is worth noting that in the limit of $Wz_0 \gg 1$ we have $T_0 \approx 1$ and hence $\sigma \approx 1$. In this regime, the above solutions can be cast into the simple forms

$$b = \exp(i\lambda z), \quad (15a)$$

$$a = \sqrt{\frac{W^2T^2(z) + \lambda^2}{\kappa_0^2}} \exp\left[i \tan^{-1}\left(\frac{WT(z)}{\lambda}\right)\right] \exp\left(i\lambda z\right), \quad (15b)$$

where in the above formula we dropped the common constant phase factor $\exp(i\lambda z_0)$. The evolution of the amplitude square is depicted in Fig. 3(a). Surprisingly, the amplitude of the lossy waveguide remains almost constant (constant in the limit $z_0 \to \infty$), while that of the gain arm experiences an intermediate appreciable loss before it is restored to its initial value. The phase advance in both channels is plotted in Fig. 3(b). At $z = -z_0$, $a/b = \exp(-i\theta)$, while $a(z_0)/b(z_0) = \exp(i\theta)$, i.e., the $\mathcal{PT}$ mode at $z = -z_0$ evolves into the $\mathcal{PT}$-symmetric

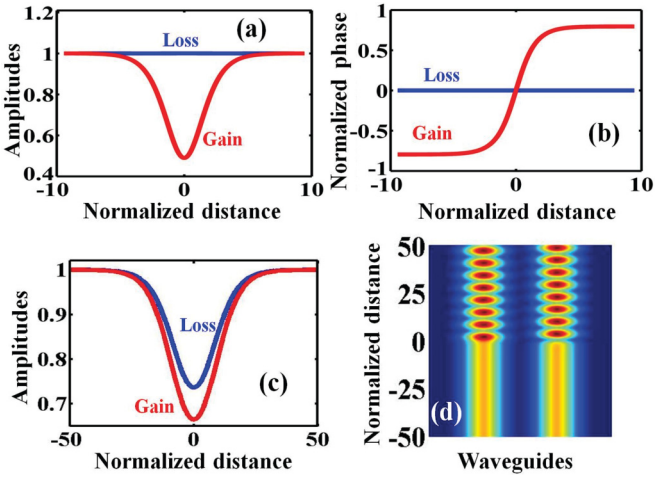

FIG. 3. (Color online) Evolution of (a) intensity and (b) phases of an input mode. Asymmetric behavior in both figures is observed with fractional phase transfer. Intensity evolution when the gain-loss profile is $\gamma(z) = 0.5 \tanh(z/10)$ and (d) top view of the intensity tunneling dynamics for rapid gain-loss variations: $\gamma(z) = 0.5 \tanh(0.9z)$. In all the above, the input was a $\mathcal{PT}$ tilted supermode. In (d), the left channel is initially experiencing loss and vice versa for the right arm.

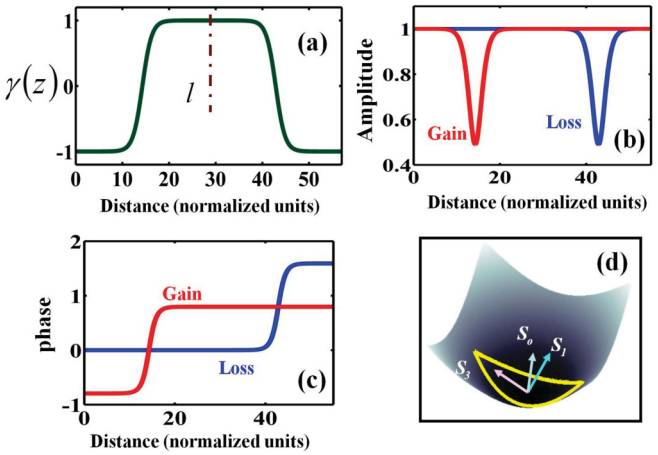

FIG. 4. (Color online) (a) One period of the periodic evolution of $\gamma(z)$ defined in the text. (b) and (c) depict the amplitude and phase dynamics indicating accumulation of net fractional phase 2θ after one complete cycle. (d) Evolution as observed in the Stokes space where trajectories live on hyperbola and trace closed curves encompassing finite areas. The curves representing light evolution in initially loss-gain channels are indicated in the figure.

eigenstate at $z = z_0$. However, a close inspection of Fig. 3(b) reveals the counterintuitive and unanticipated result of unidirectional phase exchange, i.e., in the plotted phases, measured with respect to "λz," we find the phase of the amplitude b remains constant, while that of a gradually changes from $-\theta$ to θ. The dynamics associated with intensity tunneling for slower as well as steeper gain-loss profile variations are also depicted in Figs. 3(c) and 3(d), respectively for the parameters explained in the figure caption. Note that in Fig. 3(d), the intensity evolves smoothly until the optical beam experiences a large slope gain-loss variation in the central region of the structure. In this region a sizable fraction of the input $\mathcal{PT}$ mode is transferred into another $\mathcal{PT}$ mode (in the absence of z modulation a two-dimensional $\mathcal{PT}$ coupled structure will exhibit two stationary $\mathcal{PT}$ modes) and the superposition of the two modes experiences beating, thus leading to intensity oscillations.

The fact that the phase swap of Fig. 3(b) occurs in an asymmetric fashion is a highly nontrivial result with more implications than one would initially appreciate. In order to appreciate the last statement, let us consider a situation where the gain-loss variation is periodic. A simple cyclic time variation that admits a semianalytical solution is the case when $\gamma = W\,\mathrm{sn}[W(z-l),k]$, where $\mathrm{sn}[W(z-l),k]$ is the Jacobi elliptic function. As the elliptic modulus k approaches unity, the function behaves very much like hyperbolic tangent within a certain limit. Figure 4(a) shows the z dependence of $\gamma(z)$ for this last case when $k = k_0 = 0.99999$. Evidently the function is periodic with a profile behaving like $\tanh[W(z-l/2)]$ in the range $0 < z < l$, while in the domain $l < z < 2l$ it varies as $-\tanh[W(z-3l/2)]$. Thus, this situation eventually resembles that of two reversed "tanh" profiles concatenated back to back in order to form one cycle. An approximate solution in the first half cycle is given in terms of elliptic functions as (in the regime of $Wl \gg 1$)

$$a \approx \sqrt{\frac{W^2\mathrm{SN}^2(z)+\lambda^2}{\kappa_0^2}}\exp\left[i\,\tan^{-1}\left(\frac{W\mathrm{SN}(z)}{\lambda}\right)\right]\exp(i\lambda z). \tag{16}$$

while similar to the previous case, $b = \exp(i\lambda z)$. In Eq. (16) $\mathrm{SN}(z) = \mathrm{sn}(z-l,k_0)$. Similar expressions for $a(z)$ and $b(z)$ can be written in the second half of the full period. Figure 4 depicts gain-loss variation as well as the system's dynamics in real and phase space. The evolution of the phases is plotted in Fig. 4(c). Apart from a common factor $\exp(2i\lambda l)$, the system returns to its initial state after accumulating a net fractional phase of 2θ. This result is a direct outcome of the asymmetric phase swapping. If such an exchange was symmetric for each half cycle (one channel lags by $\theta/2$ and the other advances by the same amount), the net acquired phase would have been zero. Finally Fig. 4(d) demonstrates the system's dynamics on the Stokes space. Note that this evolution takes place on a hyperbola as opposed to the spherical manifold associated with the $\gamma(z) = 0$ case. This, of course is due to the fact that the conserved quantity here is S_2 [6,8,12] instead of S_0. Evidently, the evolution in phase space traces a closed trajectory (i.e., a loop).

Note that, even under modal $\mathcal{PT}$-symmetric initial condition, the input $\mathcal{PT}$ eigenfunction does not evolve adiabatically into the output $\mathcal{PT}$-symmetric normal mode. Instead, we observe a dip in the total power of the system, indicating a mixture between the two different $\mathcal{PT}$-symmetric eigenmodes. These results are depicted in Figs. 3(a) and 4(b) and are a direct outcome of the analytical solutions presented above [Eqs. (15) and (16)]. However we would like to point out that this behavior is general and is independent of the specific details of the gain-loss variations in the intermediate stage. Even if the gain-loss profiles change adiabatically with distance, this feature will still persist. In order to illustrate the generality of this behavior, we express the field amplitudes in terms of the dynamical basis that rotates in the complex plane of the $\mathcal{PT}$-symmetric eigenfunctions:

$$[\,a\;b\,]^T = A(z)V_1(z)\exp\left(i\int_{-z_0}^{z}\lambda_1(z')dz'\right) + B(z)V_2(z) \times \exp\left(i\int_{-z_0}^{z}\lambda_2(z')dz'\right). \tag{17}$$

In Eq. (17), up to a normalization constant, $V_1(z) = \{1\;\exp[i\theta(z)]\}^T$, $V_2(z) = \{1\;-\exp[-i\theta(z)]\}^T$ and both $A(z)$ and $B(z)$ are scalar amplitudes. At any propagation distance z, $V_{1,2}(z)$ satisfy the equation $\lambda_{1,2}(z)\,V_{1,2}(z) = \Lambda(z)\,V_{1,2}(z)$, with $\Lambda(z) = \left[\begin{smallmatrix} i\gamma(z) & \kappa_0 \\ \kappa_0 & -i\gamma(z)\end{smallmatrix}\right]$. This transformation is similar to a change from a diabatic basis to adiabatic ones in the adiabatic perturbation theory, except that in our case adiabatic conditions are not imposed. Applying this change of basis to Eqs. (10), we end up with the vectorial equation $(\dot{A}V_1 + A\dot{V}_1)\exp(i\int_{-z_0}^{z}\lambda_1(z')dz') + (\dot{B}V_2 + B\dot{V}_2)\exp(i\int_{-z_0}^{z}\lambda_2(z')dz') = 0$. If we assume in the above expression that both A and B are constants, we find that $A\dot{V}_1\exp(i\int_{-z_0}^{z}\lambda_1(z')dz') + B\dot{V}_2\exp(i\int_{-z_0}^{z}\lambda_2(z')dz') = 0$. By noting that $\dot{V}_1 = [0\;i\dot{\theta}\exp(i\theta)]^T$ and $\dot{V}_2 =$

$[0\ i\dot{\theta}\exp(-i\theta)]^T$, the first component of the equation is automatically satisfied. The second one gives $B/A = -\exp[2i\theta(z)]\exp(i\int_{-z_0}^{z}[\lambda_1(z') - \lambda_2(z')]dz')$. Evidently, A and B cannot be simultaneously constant. In fact they must vary with distance (time) in order for the solution to be self-consistent. This result is an outcome of the nonorthogonal nature of $\mathcal{PT}$ eigenfunctions below symmetry-breaking phase transitions, and they become constant only if there is no variation in the gain-loss or coupling profiles. On the other hand, in a regular symmetric optical coupler, we find that $\dot{V}_{1,2} = 0$ and A as well as B turn out to be constants. In other words, this eigenfunction mixing is pertinent to local $\mathcal{PT}$-symmetric structures. It is important to emphasize that these results are general and do not depend on the details of the gain-loss variation.

IV. RESONANT PROPAGATION

In this section we explore another interesting phenomenon associated with the local $\mathcal{PT}$-invariant coupled system described by Eqs. (10). As discussed before, this arrangement is equivalent to second-order oscillators for the field amplitudes $\ddot{a} + (\kappa_0^2 - \gamma^2 + \dot{\gamma})a = 0$ and $\ddot{b} + (\kappa_0^2 - \gamma^2 - \dot{\gamma})b = 0$. In the previous section, we treated these two equations in the framework of parametric oscillations with κ_0 playing the role of the natural frequency and $\pm\dot{\gamma} - \gamma^2$ as a time-dependent variable accounting to parametric forcing. As before, here we focus our attention on coupled waveguide systems with distance-dependent variables instead of time-varying

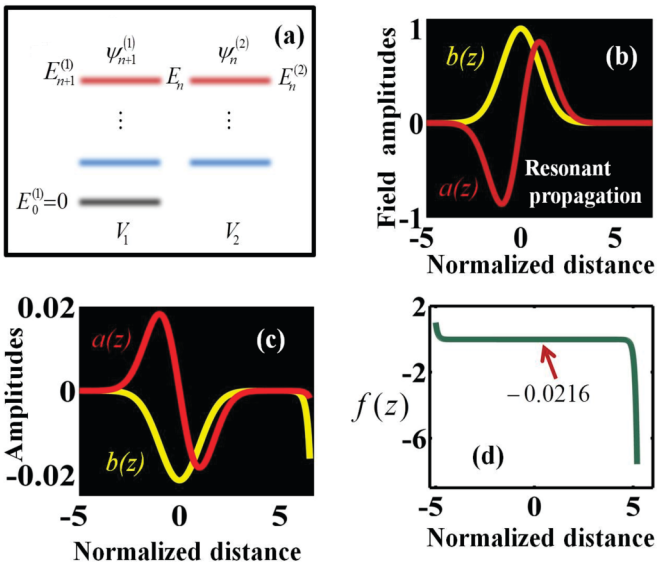

FIG. 5. (Color online) (a) Hierarchy of eigenfunctions and corresponding eigenvalues of the supersymmetric potentials. (b) Resonant propagation when the input is engineered to match the modes of the corresponding potential. (c) Resemblance of resonant propagation when the initial conditions do not coincide with the mode and numerical solution of $\int_{z'=-z_0}^{z}\psi^{-2}(z')dz'$ for the parameters explained in the text. In (b) and (c) the yellow color is the beam at the initial gain channel (one peak), while red represents intensity in the other arm (double peak curve). (d) depicts the function $f(z)$ discussed in the text.

ones [see Fig. 1(a)]. By rearranging these two equations, we get

$$-d^2a/dz^2 + (\gamma^2 - \dot{\gamma})a = \kappa_0^2 a \tag{18a}$$

$$-d^2b/dz^2 + (\gamma^2 + \dot{\gamma})b = \kappa_0^2 b. \tag{18b}$$

One can now think of these two formulas as stationary Schrödinger equations with potential given by $V_{1,2}(z) = \gamma^2 \mp \dot{\gamma}$ and an eigenvalue of κ_0^2. Evidently in this picture, κ_0^2 is not a free parameter that can take any value; instead its value will be determined by the solution of (18) under a certain choice of the potential functions. In the language of quantum mechanics, the two potentials $V_{1,2}(z)$ are called the supersymmetric partner potentials and γ is typically referred to as the superpotential. In this context, it is known that apart from one ground state, $V_{1,2}(z)$ share the same eigenvalue spectra. In some special cases where the uncommon null ground state does not exist, one says that supersymmetry is broken. The relationship between the eigenvalue spectra of both $V_{1,2}(z)$ is schematically depicted in Fig. 5(a). In order to establish the relationships between the eigenfunctions sharing the same eigenvalues, we write Eq. (18) as [23]

$$\hat{H}_1 a = \hat{A}\hat{B}a = \kappa_0^2 a, \tag{19a}$$

$$\hat{H}_2 b = \hat{B}\hat{A}b = \kappa_0^2 b, \tag{19b}$$

where $\hat{H}_{1,2} = -d^2/dz^2 + (\gamma^2 \mp \dot{\gamma})$, $\hat{A} = -d/dz + \gamma(z)$, and $\hat{B} = d/dz + \gamma(z)$. If $\psi_n^{(1)}$ satisfies $\hat{H}_1\psi_n^{(1)} = \hat{A}\hat{B}\psi_n^{(1)} = E_n^{(1)}\psi_n^{(1)}$, then it follows that $\hat{H}_2(\hat{B}\psi_n^{(1)}) = \hat{B}\hat{A}\hat{B}\psi_n^{(1)} = E_n^{(1)}(\hat{B}\psi_n^{(1)})$. In other words, if $\psi_n^{(1)}$ is the eigenfunction of $\hat{H}_1$, we find that $\hat{B}\psi_n^{(1)}$ is the corresponding (having the same eigenvalues) eigenket of $\hat{H}_2$. Similarly we can show that $\psi_n^{(2)}$ and $\hat{A}\psi_n^{(2)}$ are both eigensolutions of $\hat{H}_{2,1}$ sharing the same eigenvalues. Imposing the same normalization $\langle\psi_{n+1}^{(1)}|\psi_{n+1}^{(1)}\rangle = \langle\psi_n^{(2)}|\psi_n^{(2)}\rangle$, we finally arrive at the relationships [see Fig. 5(a)] $\psi_n^{(2)} = \hat{B}\psi_{n+1}^{(1)}/\sqrt{E_{n+1}^{(1)}}$ and $\psi_{n+1}^{(1)} = \hat{A}\psi_n^{(2)}/\sqrt{E_n^{(2)}}$ with $E_n = E_{n+1}^{(1)} = E_n^{(2)}$.

Next consider the evolution equations (19) when the coupling constant takes the value $\kappa_0 = \sqrt{E_n}$ and under the initial conditions $a(-z_0) = i\psi_{n+1}^{(1)}(-z_0)$ and $b(-z_0) = \psi_n^{(2)}(-z_0)$. By substituting in Eq. (10a), we obtain $\dot{a}(-z_0) + i\gamma(-z_0)\psi_{n+1}^{(1)}(-z_0) = i\sqrt{E_n}\psi_n^{(2)}(-z_0)$. However, from the previous analysis, we also have $d\psi_{n+1}^{(1)}/dz + \gamma(z)\psi_{n+1}^{(1)}(z) = \sqrt{E_n}\psi_n^{(2)}(z)$. By comparing the last two equations together we find that $\dot{a}(-z_0) = id\psi_{n+1}^{(1)}/dz|_{z=-z_0}$. Similar considerations show that $\dot{b}(-z_0) = d\psi_n^{(2)}/dz|_{z=-z_0}$. In other words, for a specific chosen coupling constant [being an eigenvalue of Eqs. (18) or equivalently, Eq. (19)] and by matching the initial conditions to those of the corresponding eigenfunctions, it is ensured that the initial values of the field amplitude derivatives will coincide with those of the eigenmodes of Eqs. (19). Thus under these initial excitations, the dynamics of the amplitudes $a(z)$ and $b(z)$ will follow exactly the functional form of $\psi_{n+1}^{(1)}$ and $\psi_n^{(2)}$—a process that we call resonant propagation.

In order to elucidate this point, let us consider a concrete example. Assuming $\gamma(z) = z$, it follows that $V_{1,2}(z) = z^2 \mp 1$. One can easily check that the first two eigenfunctions of $V_1(z)$ are $\psi_0^{(1)} = \exp(-z^2/2)$ and $\psi_1^{(1)} = 2z\exp(-z^2/2)$ with

eigenvalues of $E_0^{(1)} = 0$ and $E_1^{(1)} = 2$. On the other hand, the ground state of $V_2(z)$ is given by $\psi_0^{(2)} = \exp(-z^2/2)$ with $E_0^{(2)} = 2$. Thus, if the numerical value of the coupling constant in Eq. (1) is $\kappa_0 = \sqrt{2}$ and the initial input field amplitudes are $a(-z_0) = -i\sqrt{2}z_0 \exp(-z_0^2/2)$ and $b(-z_0) = \exp(-z_0^2/2)$, it will follow that the beam evolution at any location z is given by $a(z) = i\sqrt{2}z \exp(-z^2/2)$ and $b(z) = \exp(-z^2/2)$. In order to verify these results, Eqs. (10) are numerically integrated under these specific initial inputs and excellent agreement with the mode profiles is obtained [see Fig. 5(b)]. Here as well as below, we take $z_0 = 5$.

It is important to make few comments here. First we note that in spite of the existence of a linear gain-loss profile, the field amplitudes in both channels die out at the output and that would still be the case even if the local $\mathcal{PT}$ symmetry were broken, i.e., even if $\gamma(z) > \kappa_0 = \sqrt{2}$ at any specific range of z. Second, it is interesting to observe that in the specific case under consideration, the fields propagate in both arms without accumulating any phase at all, not even a dynamical one. Another interesting observation is that even when the input does not satisfy the supermode initial condition, we find that field amplitude evolution still resides on a scaled version of the modes before it blows up eventually. For example, Fig. 5(c) shows the dynamics when $a(-z_0) = 0$ and $b(-z_0) = \exp(-z_0^2/2)$. Apart from a scaled factor of -0.0215, the displayed dynamics in Fig. 5(c) resembles that of Fig. 5(b) for some propagation distance range before the amplitudes start to grow up unboundedly at around $z = 5$. In order to understand this behavior, we investigate the dynamics of Eq. (18b) under nonmodal excitations. We assume that the initial conditions are given by $b(-z_0) = C_1$ and $\dot{b}(-z_0) = C_2$. Furthermore, we use the ansatz $b(z) = f(z)\,\psi(z)$, where $\psi(z)$ is the eigenmode that satisfies Eq. (18b) with eigenvalue κ_0^2. Substituting in (18) immediately yields $f_{zz}(z)\,\psi(z) + 2f_z\psi_z = 0$. Integrating once gives $f_z(z) = \chi_1\psi^{-2}(z)$ and finally we find that $f(z) = \int f_z(z)\,dz = \chi_1 \int_{z'=-z_0}^{z} \psi^{-2}(z')dz' + \chi_2$, where $\chi_{1,2}$ are the constants of integration. Note that $f(-z_0)\psi(-z_0) = \chi_2\psi(-z_0) = C_1$, hence it only remains to find the value of χ_1. From the second initial condition, we get $(f_z\psi + f\psi_z)|_{z=-z_0} = C_2$, which upon substitution gives $\chi_1\psi^{-2}(-z_0)\psi(-z_0) + \chi_2\psi_z(-z_0) = C_2$ or $\chi_1 = \psi(-z_0)[C_2 - \chi_2\psi_z(-z_0)]$. For the specific example depicted in Fig. 5(c), $\psi(z) = \exp(-z^2/2)$, $C_1 = \exp(-z_0^2/2) = \psi(-z_0)$, and $C_2 = z_0\exp(-z_0^2/2) = -\psi_z(-z_0)$. Substituting back, we find that $\chi_2 = 1$ and $\chi_1 = -2\psi(-z_0)\psi_z(-z_0) = -10\exp(-25)$. Finally $f(z)$ can be determined by using the values of $\chi_{1,2}$ and performing the integral $\int_{z'=-z_0}^{z} \psi^{-2}(z')dz'$ numerically in the range of interest, which we choose here to be $-5 < z < 5.2$. The result of this integration is shown in Fig. 5(d). It is evident that the function is flat over most of the range except from the very beginning and close to $z = 5$. This result shows that initial values of $f(z)$ compensate for the discrepancy between the initial conditions and the mode profiles and after a short propagation distance, the fields adjust to a scaled version of the eigenmodes. In the flat range centered around $z = 0$, we find that $f(z = 0) \approx -0.0215$, which accounts for the observed scaling between Figs. 5(b) and 5(c). Finally we note that shortly after $z = 5$, the function $f(z)$ starts to blow up, thus explaining the behavior of the fields in this range as shown in Fig. 5(c). This analysis cannot be applied in a straightforward manner to Eq. (18a). However, one can infer the result by noting that the two fields in both arms are coupled and that a modal evolution of one implies the same for its partner, which is confirmed using numerical solutions of Eqs. (10) as depicted in Fig. 5(c). It is worth noting that for the particular harmonic oscillator potential, Eq. (18a) can be reduced to the Hermite differential equation that exhibits an analytical solution; however, for a general potential, such solutions might not exist and one has to resort to analyzing the ground state of Eq. (18b) in order to gain insight into the system's behavior. The question that naturally arises at this point is, what happens if the coupling constant was chosen to coincide with the eigenvalues of higher excited modes that do not include any ground state? Numerical simulations show that under these conditions the input still demonstrates resonant propagation before it blows up. How can one understand this result given that the previous analysis cannot be systematically carried on for any other state than the ground state? Here also one can use the machinery of supersymmetry to simplify the situation as depicted in Fig. 6. For concreteness, assume the coupling constant matches the eigenvalue of the third and second excited modes of potentials V_1 and V_2, respectively, i.e., $\kappa_0^2 = E_2^{(2)} = E_3^{(1)}$. Equation (18b) can then be rewritten as $-d^2b/dz^2 + (\gamma^2 + \dot{\gamma} - E_0^{(2)})b = (\kappa_0^2 - E_0^{(2)})b$. In this modified form, a new potential $V_3 = \gamma^2 + \dot{\gamma} - E_0^{(2)}$ with null eigenvalue ground state can be identified. By constructing the superpartner potential of V_3, call it V_4, the dynamics of b can be coupled to that of the field amplitude described by V_4. Noteworthy, the second-order mode of V_3 corresponds to a well-behaved ground state of V_4 and thus the previous analysis can be carried on and then mapped back to b and finally to a. Figure 6 shows a schematic for building such a hierarchy of SUSY potentials.

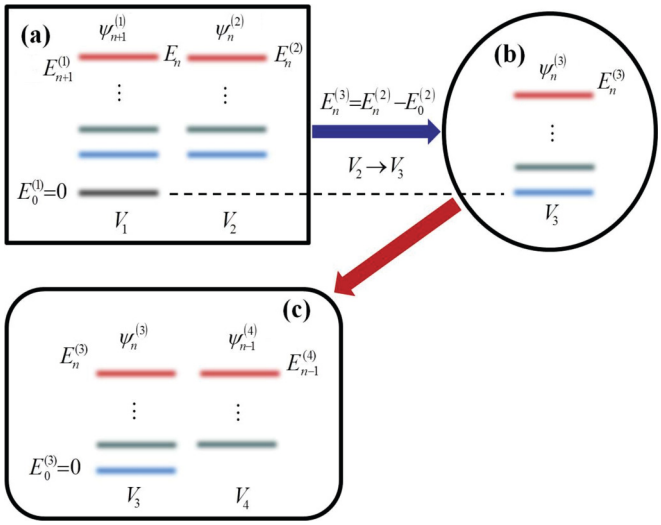

FIG. 6. (Color online) Schematic of building up a sequence of SUSY potentials: (a) structure of eigenvalues of the first two supersymmetric potentials; (b) shifting down the levels of the second potential in order for it to exhibit a zero ground state (without affecting the dynamical evolution); and (c) building its SUSY partner.

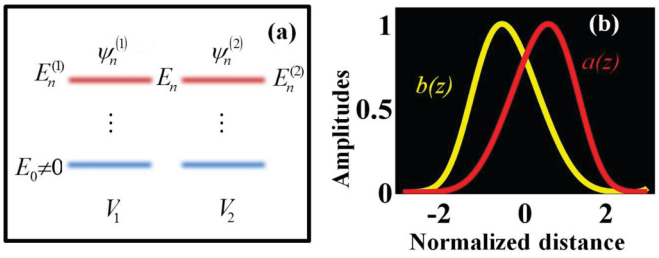

FIG. 7. (Color online) Broken SUSY is depicted in (a) and its manifestation in the input beam evolution (b). Note that in this case the same number of peaks (one in this situation) is shared by beams in both arms. Colors indicate the same as in Figs. 5(b) and 5(c).

So far we have considered a case of unbroken SUSY. This is characterized by the existence of a ground state with null eigenvalues for one of the potentials. Note also that SUSY links one eigenfunction of one potential to another (of the other superpotential) that differs from it by only one node. Mathematically, unbroken SUSY can be investigated using the Witten index defined as [26] $W = \lim_{\beta\to 0} \int (dp\, dz/2\pi) \exp[-\beta(p^2/2) + \gamma^2/2](\beta\gamma_z/2)$. When $W = 1$, the supersymmetry is unbroken as in the previous case of $\gamma = z$. However, in the case where $W = 0$, SUSY is broken and the system is characterized by the absence of a zero eigenvalue ground state. Under this condition, the eigenvalues and eigenfunctions of the superpotentials are linked via $\psi_n^{(2)} = \hat{B}\psi_n^{(1)}/\sqrt{E_n^{(1)}}$ and $\psi_n^{(1)} = \hat{A}\psi_n^{(2)}/\sqrt{E_n^{(2)}}$, and $E_n = E_n^{(1)} = E_n^{(2)}$. This scenario is depicted in Fig. 7(a). A typical example of a gain-loss profile that will correspond to broken SUSY is $\gamma(z) = z^2$. It is easy to check that for this case, the Witten index is zero, thus indicating broken symmetry. The superpotentials under these conditions are given by $V_{1,2}(z) = z^4 \pm 2z$. Figure 7(b) shows the behavior of input beam evolution under these conditions where it is evident that only one peak (in each arm) exists as expected from broken supersymmetry.

V. CONCLUSIONS

In conclusion, we introduced the concept of local parity-time reversal symmetry where even index guiding and odd gain-loss symmetry is preserved locally while gain-loss profiles vary with time or distance. Starting from a Lagrangian description of PO, we have established the mathematical connection between local $\mathcal{PT}$ symmetry and PO. Using this analogy, we have shown that the conservation of the quantity often termed quasipower (in the context of $\mathcal{PT}$ symmetry) is a direct outcome of the global gauge invariance of the system's Lagrangian.

We have studied a particular local $\mathcal{PT}$ coupled configuration where analytical solutions can be obtained via the parametric oscillation equivalence. Depending on the configuration under investigation and on the input initial conditions, the system was shown to exhibit a host of intriguing behaviors, ranging from nondynamical fractional phase exchange to resonant propagation. Under fractional phase exchange conditions, an input $\mathcal{PT}$ mode will experience a unidirectional phase accumulation, while the mode is changing its tilt direction during evolution. This asymmetric phase exchange results in a total nondynamical phase factor after one cycle of evolution (in the case of periodic gain-loss distributions).

Our analysis also pointed out an intriguing connection between local $\mathcal{PT}$ coupled systems and SUSY symmetry. In particular, under resonant propagation conditions (defined in Sec. IV), a tailored input beam was shown to propagate "residing" on the eigenmodes of the corresponding stationary Schrödinger equation. Depending on the gain-loss profile, supersymmetry can be broken or not. These properties are manifested in the dynamics via the appearance of an extra peak in one arm for unbroken SUSY.

ACKNOWLEDGMENTS

We would like to thank Professor Ewan Wright, University of Arizona and Dr. Mohamed Anber, University of Toronto for their fruitful discussions and insightful comments. This work was also supported by NSF grant ECCS-1128520 and by AFOSR grant FA95501210148.

[1] C. M. Bender and S. Boettcher, Phys. Rev. Lett. **80**, 5243 (1998).
[2] C. M. Bender, Phys Rep. Prog. Phys. **70**, 947 (2007).
[3] A. Znojil, Phys. Lett. A **285**, 205 (2001).
[4] Z. Ahmed, Phys. Lett. A **282**, 343 (2001).
[5] R. El-Ganainy, K. G. Makris, D. N. Christodoulides, and Z. H. Musslimani, Opt. Lett. **32**, 2632 (2007).
[6] K. G. Makris, R. El-Ganainy, D. N. Christodoulides, and Z. H. Musslimani, Phys. Rev. Lett. **100**, 103904 (2008).
[7] K. G. Makris, R. El-Ganainy, D. N. Christodoulides, and Z. H. Musslimani, Phys. Rev. A **81**, 063807 (2010).
[8] K. G. Makris, R. El-Ganainy, D. N. Christodoulides, and Z. H. Musslimani, Int. J. Theor. Phys. **50**, 1019 (2011).
[9] Z. H. Musslimani, K. G. Makris, R. El-Ganainy, and D. N. Christodoulides, Phys. Rev. Lett. **100**, 030402 (2008); J. Phys. A: Math. Theor. **41**, 244019 (2008).
[10] A. Guo, G. J. Salamo, D. Duchesne, R. Morandotti, M. Volatier-Ravat, V. Aimez, G. A. Siviloglou, and D. N. Christodoulides, Phys. Rev. Lett. **103**, 093902 (2009).
[11] C. E. Ruter, K.G. Makris, R. El-Ganainy, D.N. Christodoulides, M. Segev, and D. Kip, Nat. Phys. **6**, 192 (2010).
[12] H. Ramezani, T. Kottos, R. El-Ganainy, and D. N. Christodoulides, Phys Rev. A **82**, 043803 (2010).
[13] N. Moiseyev, Phys. Rev. A **83**, 052125 (2011).
[14] M.V. Berry and R. Uzdin, J. Phys. A: Math. Theor. **44**, 435303 (2011).
[15] V. S. Shchesnovich and V. V. Konotop, Phys. Rev. A **81**, 053611 (2010).
[16] V. Leroy, J. C. Bacri, T. Hocquet, and M. Devaud, Eur. J. Phys. **27**, 469 (2006).

[17] W. B. Case and M. A. Swanson, Am. J. Phys. **58**, 463 (1990).
[18] W. B. Case, Am. J. Phys. **64**, 215 (1996).
[19] R. E. Collin, *Foundations for Microwave Engineering*, 2nd ed. (Wiley-IEEE Press, 2000).
[20] C. L. Tang and L. K Cheng, *Fundamentals of Optical Parametric Processes and Oscillations*, 1st ed. (Harwood Academic Press, 1995).
[21] Y. V. Kartashov, L. Torner, and V. A. Vysloukh, Opt. Lett. **29**, 1102 (2004).
[22] M. Devaud, V. Leroy, J.-C Bacri, and T. Hocquet, published on http://hal.archives-ouvertes.fr/docs/00/19/75/65/PDF/Adiabatic_Invariant.pdf.
[23] C. V. Sukumar, J. Phys. A **18**, L56 (1985).
[24] F. Cooper and B. Freedman, Ann. Phys. **146**, 262 (1983).
[25] Dwight E. Neuenschwander, *Emmy Noether Wonderful Theorem*, 1st ed. (The Johns Hopkins University Press, Baltimore, 2010).
[26] E. Witten, Nucl. Phys. B **202**, 253 (1982).